

Penumbra lunar eclipse observations reveal anomalous thermal performance of Lunakhod 2 reflectors

Tian-Quan Gao(高添泉), Cai-Shi Zhang(张才士), Hong-Chao Zhao(赵宏超), Li-Xiang Zhou(周立祥), Xian-Lin Wu(吴先霖), Hsienchi Yeh(叶贤基), and Ming Li(李明)

Citation: Chin. Phys. B, 2022, 31 (**5**): 050602. DOI: 10.1088/1674-1056/ac3068
Journal homepage: http://cpb.iphy.ac.cn; http://iopscience.iop.org/cpb

What follows is a list of articles you may be interested in

Fiber-based joint time and frequency dissemination via star-shaped commercial telecommunication network

Yi-Bo Yuan(袁一博), Bo Wang(王波), Li-Jun Wang(王力军)
Chin. Phys. B, 2017, 26 (**8**): 080601. DOI: 10.1088/1674-1056/26/8/080601

Fiber-based multiple access timing signal synchronization technique

Yi-Bo Yuan(袁一博), Bo Wang(王波), Chao Gao(高超), Li-Jun Wang(王力军)
Chin. Phys. B, 2017, 26 (**4**): 040601. DOI: 10.1088/1674-1056/26/4/040601

Fiber-based multiple-access frequency synchronization via 1f-2f dissemination

Xi Zhu(朱玺), Bo Wang(王波), Chao Gao(高超), Li-Jun Wang(王力军)
Chin. Phys. B, 2016, 25 (**9**): 090601. DOI: 10.1088/1674-1056/25/9/090601

In-situ multi-information measurement system for preparing gallium nitride photocathode

Fu Xiao-Qian,Chang Ben-Kang,Qian Yun-Sheng,Zhang Jun-Ju
Chin. Phys. B, 2012, 21 (**3**): 030601. DOI: 10.1088/1674-1056/21/3/030601

Penumbra lunar eclipse observations reveal anomalous thermal performance of Lunakhod 2 reflectors

Tian-Quan Gao(高添泉), Cai-Shi Zhang(张才士), Hong-Chao Zhao(赵宏超), Li-Xiang Zhou(周立祥), Xian-Lin Wu(吴先霖), Hsienchi Yeh(叶贤基), and Ming Li(李明)†

MOE Key Laboratory of TianQin Mission, TianQin Research Center for Gravitational Physics & School of Physics and Astronomy, Frontiers Science Center for TianQin, CNSA Research Center for Gravitational Waves, Sun Yat-sen University (Zhuhai Campus), Zhuhai 519082, *China*

(Received 26 August 2021; revised manuscript received 8 October 2021; accepted manuscript online 18 October 2021)

As the signal reflected by the corner-cube reflector arrays is very weak and easily submerged during the full moon, we analyze the influence of the thermal effect of corner-cube reflector arrays on the intensity of lunar laser ranging echo. Laser ranging measurements during the penumbra lunar eclipse verify suspected thermal deformation in the Lunakhod 2 reflectors. Signal levels vary over two orders of magnitude as the penumbra eclipse progresses. This can be explained by the change in the dihedral angle of the corner-cube reflectors caused by the temperature. The results show that when the dihedral angle errors reach $1''$, the energy is reduced by 100 times compared with the ideal corner-cube reflector. In the experiment, our findings suggest that when the corner-cube reflector arrays enter the penumbra of the earth, the effective echo signal level which reaches 0.18 photons/s far exceeds the historical level of the full moon. However, 11 minutes after the penumbra lunar eclipse, the effective echo rate of Lunakhod 2 will drop two orders of magnitude. The mechanism can explain the acute signal deficit observed at full moon.

Keywords: lunar laser ranging, corner-cube reflector arrays, dihedral angle errors, penumbra lunar eclipse

PACS: 06.30.–k, 07.07.Df, 07.60.–j **DOI:** 10.1088/1674-1056/ac3068

1. Introduction

The lunar laser ranging (LLR) data is of great scientific significance. It can be used to verify the relativistic equivalence principle,[1,2] the invariability of light speed and post-Newtonian gravity.[3] Alley[4] proposed to place the corner-cube reflector arrays (CCRs) on the surface of the moon to carry out LLR experiment. On July 21, 1969, the CCRs were placed on the moon surface at predetermined position, and then the U.S. Lick Observatory[5] successfully observed the laser ranging echo signal from the Apollo 11 reflectors with 3 m telescope. On August 30, the 2.7 m telescope of the McDonald Observatory[6] in the U.S. also received echo signals. Following that, the Pic du Midi Observatory (France) and the Tokyo Observatory (Japan) successfully reached the echo signal from these reflectors.[4] Scientists at Yunnan Observatories successfully achieved LLR at 532 nm, which is the first time to measure the distance between the earth and the moon in China.[7] Apart from the Apollo 11 CCRs, there were also Apollo 14, Apollo 15, Lunakhod 1 and Lunakhod 2 (L2) reflector arrays, while the Lunakhod 1 was only received by the former Soviet Union's Crinean Observatory (2.6 m telescope) and the French Pic du Midi Observatory (1.06 m telescope) at the beginning of its placement.[8]

During the process of laser ranging, there are many factors affecting the number of photoelectrons in the echo detection, such as earth–moon distance, atmospheric transmittance, CCR reflection area, divergence angle and reflection efficiency. Two problems were identified when Murphy and other scientists carried out LLR observations.[9–15] The signal strength returned from CCRs was about ten times lower than the theoretical prediction calculated value, and the effective echo signal intensity of the CCRs was further reduced when the moon phases were within 20° of a full moon. Scientists from different countries have analyzed the attenuation of the LLR effective echo during the full moon. For example, Goodrow and Murphy[16] analyzed the influence of temperature upon energy distribution of the far-field diffraction pattern (FFDP), and suggested that the central intensity of the FFDP emerging from the CCRs was severely diminished when differences of even a few degrees of Kelvin existed across CCRs, but they did not give the effect of far-field diffraction energy on the number of echo photons received, and the effect of dihedral angle errors on FFDP was not described. Murphy[17] used a lunar eclipse to conduct the LLR experiment and investigated the effect of temperature on the effective echo intensity of the Apollo CCRs, but they did not analyze Lunakhod 2 reflectors. Then, in order to increase the efficiency of LLR, a next-generation single lunar CCR was developed by Currie.[18] Martini[19] focused on its thermal influence upon the energy distribution of the FFDP. Otsubo,[20] Zhou,[21] and He[22] also examined the effect of the dihedral angle errors on the far-field diffraction energy distribution, but they did not do space experiments.

Because of the special position of L2, the data of L2 can be used to study the lunar libration more effectively. The study of L2 is of great significance. The goal of this paper is to build up a model and analyze the effect of dihedral angle errors of

†Corresponding author. E-mail: liming73@mail.sysu.edu.cn

© 2022 Chinese Physical Society and IOP Publishing Ltd

L2 on FFDP. We interpret the complex amplitude distribution of the output beam caused by dihedral angle errors of a non-ideal CCR based on the geometry of the CCR. LLR experiments which use superconducting nanowire single photon detectors (SNSPDs) at 1064 nm wavelength are conducted during a penumbral eclipse. This is the first time that SNSPDs are used for LLR. In our research, LLR experiment is performed on the CCRs of L2 during the penumbra lunar eclipse period. Based on data processing, it concludes that the effective echo intensity of L2 is sensitive to dihedral angle errors changed.

2. LLR system

The LLR system has been designed and installed at Zhuhai, as shown in Fig. 1. The system consists of electrical system and optical system. The optical system is divided into imaging tracking system and echo photon receiving system. The LLR system with the newly fabricate SNSPDs is shown in Fig. 2(a). As the performance of SNSPDs is much better than that of avalanche photodiode (APD) at infrared wavelengths, our system using SNSPDs at 1064 nm wavelength is more promising to obtain higher detection efficiency and a higher signal to noise ratio. A telescope, as shown in Fig. 2(b), with a diameter of 1.2 m, is used not only to emit laser but also to receive photons which are reflected by the target. Another important equipment in the ranging system is the high repetitive, picosecond pulse laser. Researchers at Shanghai Institute of Optics and Fine Mechanics obtained a single energy of 10 mJ with a pulse width of 13 ns at a pulse repetition rate of 250 Hz at 1064 nm.[23] Shanghai Astronomical Observatory used a 60 W nanosecond green laser at 200 Hz for debris laser ranging.[24] In this paper, a laser with wavelength of 1064 nm, a pulse width of 80 ps, a repetition frequency of 100Hz and a single pulse energy of 300 mJ is used, as shown in Fig. 2(c).

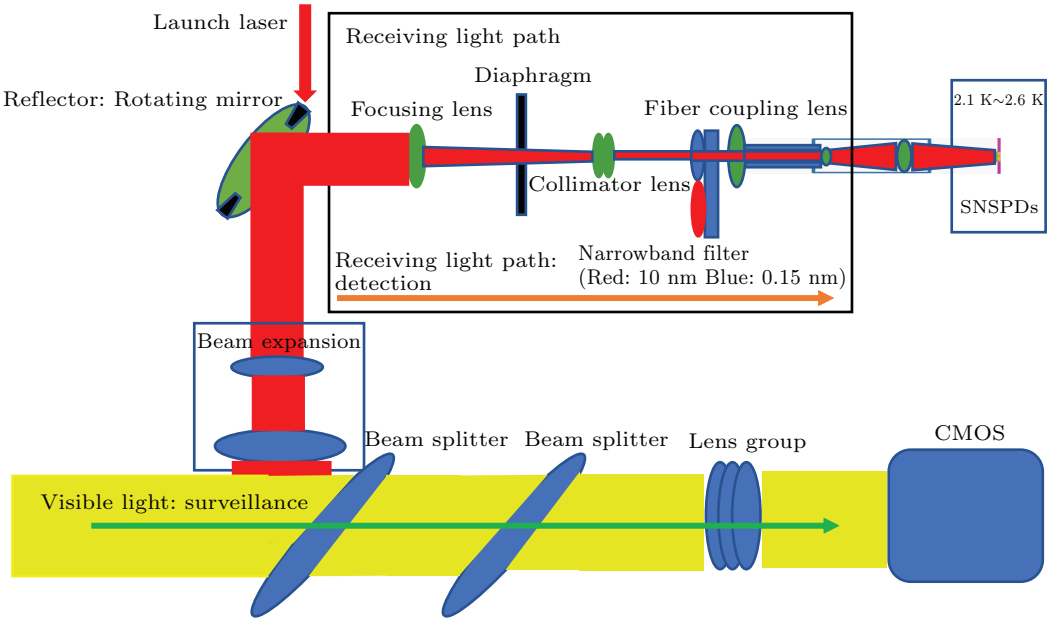


Fig. 1. LLR system. Laser transmission and reception are switched by the rotating mirror. Two kinds of filters with bandwidth of 0.15 nm and 10 nm are used for background suppression. Small field of view imaging camera is used to image the target and achieve high precision pointing.

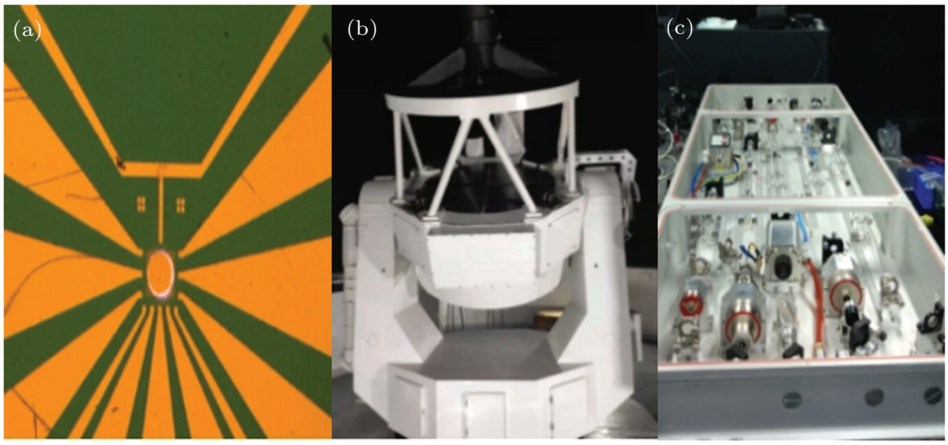


Fig. 2. (a) SNSPDs. SNSPDs with an intrinsic quantum efficiency of 80% and a dark count rate of 100 cps at 1064 nm wavelength are developed and introduced to TianQin laser ranging observatory in China. (b) 1.2 m laser ranging telescope. Co-axis-aperture laser ranging telescope. The telescope carries out high-precision tracking of the target with a pointing accuracy of $2''$. (c) Laser with 1064 nm wavelength, 300 mJ single pulse energy, 80 ps laser pulse width and 100 Hz repetition frequency.

Compared with 532 nm, the usage of 1064 nm wavelength in LLR help to achieve high atmospheric transmittance and larger number of photons contained under the same energy condition. Then compared with the Grasse observatory, a higher repetition rate laser is used in this experiment to improve the detection signal-to-noise ratio of the system. Compared with Apache observatory, we used SNSPDs[25–27] for LLR to improve detection probability.

3. Thermal analysis of CCRs

The effect of temperature will introduce additional phase, shown as[16]

$$\Delta\phi = \frac{2\pi l'}{\bar{\lambda}} = \frac{2\pi l\,(1+\alpha\delta\bar{T})\,(n_0+\beta\delta\bar{T})}{\lambda_0}, \tag{1}$$

where λ_0 is the vacuum wavelength, n_0 is the refractive index, δT is departure from some reference temperature, β is thermo-optic coefficient, α is the thermal expansion coefficient, and l is geometric path length.

CCRs of Apollo are designed with specialized shading structures, but L2 does not have such structures, making it more susceptible to environmental influences. We consider that temperature changes will produce dihedral angle errors. There are three dihedral angle errors in the CCRs when they are heated, which cause changes of the additional vector of the beam distribution of the outgoing light field. The additional vector $\mathrm{d}F$ of the reflected beam after three reflections from the reflective surface of the reflectors is calculated when there are three dihedral angle errors, and the coordinate system of the corner reflector is established as described in reference[21]

$$\begin{aligned}
\mathrm{d}F_1 &= \big[2(A_2\delta_1+A_3\delta_2),2(A_3\delta_3-A_1\delta_1),\\
&\quad -2(A_2\delta_3+A_1\delta_2)\big]^{\mathrm{T}},\\
\mathrm{d}F_2 &= \big[2(A_3\delta_2+A_2\delta_1),-2(A_3\delta_3+A_1\delta_1),\\
&\quad 2(A_2\delta_3-A_1\delta_2)\big]^{\mathrm{T}},\\
\mathrm{d}F_3 &= \big[2(A_3\delta_2-A_2\delta_1),2(A_1\delta_1+A_3\delta_3),\\
&\quad -2(A_1\delta_2+A_2\delta_3)\big]^{\mathrm{T}},\\
\mathrm{d}F_4 &= -\mathrm{d}F_2,\quad \mathrm{d}F_5=-\mathrm{d}F_3,\quad \mathrm{d}F_6=-\mathrm{d}F_1,
\end{aligned} \tag{2}$$

where δ_1, δ_2 and δ_3 are the dihedral angle errors between two pairs of the three reflecting surfaces of the reflectors, and A is the refraction vector.

After the additional vector of the reflected beam is refracted through the bottom surface of the CCR, the additional vector $\mathrm{d}R_m$ of the laser beam is emitted, which can be calculated as

$$\begin{aligned}
&\mathrm{d}R_m = [\mathrm{d}R_{mx},\mathrm{d}R_{my},\mathrm{d}R_{mz}]^{\mathrm{T}} = \mathrm{refr}\,(\mathrm{d}F_m,-N_0),\\
&m=1,2,3,\ldots,6,
\end{aligned} \tag{3}$$

where N_0 is the normal direction of the bottom surface of the reflector.

The additional optical path of the outgoing laser beam caused by the dihedral angle errors are calculated to satisfy the following relation:

$$\begin{aligned}
&\omega\alpha_m = -\sqrt{2}r\tan\alpha\,(\mathrm{d}R_{mx}\cos\theta+\mathrm{d}R_{my}\sin\theta),\\
&m=1,2,3,\ldots,6,
\end{aligned} \tag{4}$$

where r is the radius of the bottom surface, θ is the azimuth angle of the incident laser beam in the base plane coordinate system of reflectors and α is the refraction angle of the incident laser beam at the bottom surface.

Calculate the far-field diffraction intensity of the laser beam reflected by the CCR,[21] and the additional phase will change the energy distribution of FFDP

$$I = \frac{\cos^2\phi}{\lambda_{\mathrm{r}}^2 d_0^2}\cdot\left|\iint_A |E|\exp\left(-\mathrm{i}k\frac{x'x'_{\mathrm{r}}+y'y'_{\mathrm{r}}}{\rho_0}\right)\mathrm{d}x'\,\mathrm{d}y'\right|^2, \tag{5}$$

$$E = |E|\exp\left[\mathrm{i}\frac{2\pi}{\lambda_{\mathrm{r}}}(\omega\alpha_m)\right], \tag{6}$$

where λ_{r} is the laser wavelength, A is effective diffraction region which depends on the aperture of the CCR, k refers to the wave number and E represents the complex amplitude of the reflected beam. The other parameters in the formula can be referred to reference.[21]

When the specifications of the system parameters are given, the received photon number can be directly derived from the FFDP of the CCR. According to the radar equation, the received photon number of the LLR system can be given by

$$\begin{aligned}
n &= \eta_{\mathrm{q}}\left(E_{\mathrm{T}}\frac{\lambda}{hc}\right)b_{\mathrm{t}}\sigma\left(\frac{1}{4\pi R^2}\right)^2\\
&\quad\times A_{\mathrm{r}}b_{\mathrm{r}}T_{\mathrm{a}}^2\cdot I\cdot\eta_{\mathrm{pointing}}\cdot\eta_{\mathrm{turbulence}},
\end{aligned} \tag{7}$$

where R is the range from the target to the observation station, λ is the laser wavelength, h is Planck's constant, c is the light speed, E_{T} is the pulse energy, T_{a} is the atmospheric transmittance, σ is the total cross section of the retroreflectors, A_{r} is the aperture of the receiving telescope, b_{t} and b_{r} are the optical system efficiencies of the transmitting and receiving systems, η_{pointing} is the attenuation coefficient of pointing error, $\eta_{\mathrm{turbulence}}$ is the attenuation coefficient of atmospheric turbulence, and η_{q} is the quantum efficiency. Diffraction spot energy directly affected the number of effective echo photons.

4. Energy distribution of FFDP of CCRs

The effective echo intensity received by the ground station from the CCRs is not only related to the detection performance of the system, but also is mainly affected by the energy distribution of the FFDP of CCRs, as shown in Eq. (7). The dihedral angle errors designed of standard CCRs are 0° to get

higher energy without any extra phase difference. The FFDP energy distribution is analyzed without dihedral angle errors, as shown in Fig. 3. The FFDP of a standard CCR presented a circular distribution with the strongest central energy and relatively weak surrounding energy. Goodrow analyzed effect of the temperature gradient on the diagonal reflection of far-field energy, and he thought that the expansion coefficient of Apollo reflector was small, so the influence of this part was ignored. However, the L2 is not designed to block light, so temperature changed have a significant influence on the deformation of the dihedral angle. Here we intend to focus on the analysis of dihedral angle errors which are caused by temperature, and calculate the far-field energy distribution.

The aberration caused by the measured target is an important factor affecting the amount of echo energy the station receive, as shown in Fig. 3. The range of aberration involved in LLR is 3.5 μrad–7 μrad. The red circle in Fig. 3 represents the far-field energy corresponding to a velocity aberration of 3.5 μrad. The energy intensity at aberration of 3.5 μrad is about 3 times of that of 7 μrad.

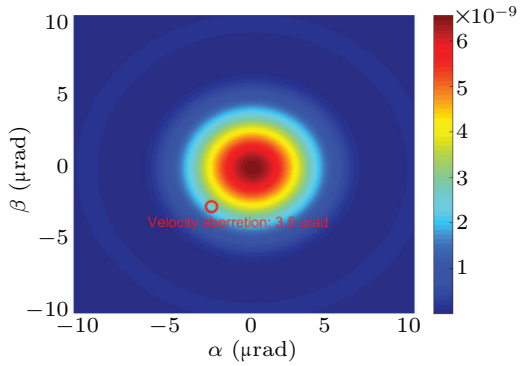


Fig. 3. The energy distribution of the FFDP when CCRs have no dihedral angle errors. The red circle indicate the target velocity aberration which reaches 3.5 μrad.

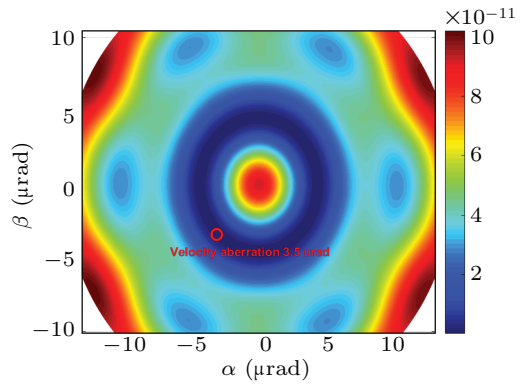


Fig. 4. The energy distribution of the FFDP when CCRs have the dihedral angle errors. The dihedral angle errors are 1″, 1″ and 1″, respectively.

Influenced by the temperature, CCRs undergo thermal deformation, which is reflected in the dihedral angle errors. It is found that the FFDP is deformed and the energy distribution appeared to separate. The effective echo intensity accepted by the station decreased sharply, as shown in Fig. 4. When the dihedral angle errors caused by temperature change are the factor to be taken into consideration with the three dihedral angle errors reaching 1″, 1″ and 1″ respectively, the energy is reduced by 2 orders of magnitude at the 3.5 μrad aberration, compared with ideal CCR.

The influence of temperature on the dihedral angle errors of the CCRs is a dynamic process, so the energy distribution of the CCRs with different dihedral angle errors is simulated in this paper, as shown in Fig. 5. In the range of velocity aberration (3.5 μrad–7 μrad), the larger the dihedral angle errors, the smaller the energy. When the velocity aberration is 3.5 μrad, the energy will be reduced by a factor of 100 times when the dihedral angle errors change from 0″ to 1″.

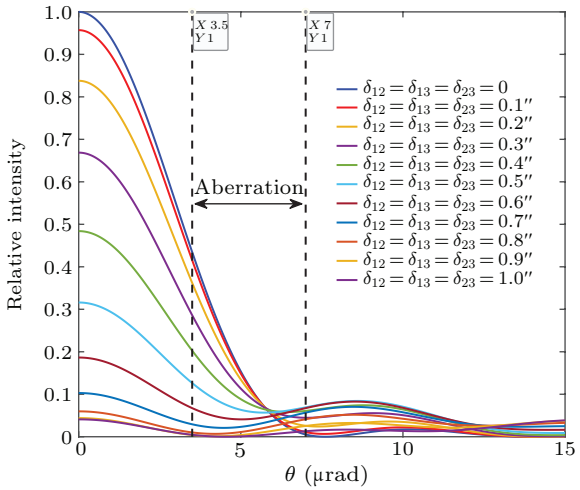


Fig. 5. The relative intensity of CCRs. The x-coordinate represents the velocity aberration, and the vertical axis is energy intensity.

5. LLR experiment

The moon entered the penumbra of the earth on November 30, 2020 and we carried out the LLR experiment on the L2 during this period. Since the CCRs of A11, A14, A15 and L1 were no longer in the penumbra of the earth at the time of the experiment, the analysis was not performed here. Table 1 records the time information of the start and end of the penumbra lunar eclipse. The penumbra lunar eclipse started at 15:30 pm on November 30 (Beijing time) and ended at 19:56 pm. The whole process lasted for 4 hours and 26 minutes. The LLR system in TianQin station is used to carry out the experiment. The system parameters are shown in Table 2.

Table 1. Penumbra lunar eclipse timetable.

Data	Time of Beijing	Status	Penumbra eclipse
2020.11.30	15:30	Start	0.855
	17:43		
	19:56	End	

Table 2. System parameters.

Parameters	Estimated value	Observed value	Comments
λ	1064 nm	1064±0.2 nm	laser wavelength
E_t	30 mJ	300 mJ–320 mJ	laser pulse energy
r_{pulse}	100 Hz	100 Hz	laser pulse repetition rate
D_t	1.2 m	/	aperture of the transmitting telescope
D_r	1.2 m	/	aperture of the receiving telescope
θ_{laser}	2″	2″–3″	laser divergence angle
θ_{track1}	2″	2″	pointing error of transmitting telescope
θ_{track2}	2″	2″	pointing error of receiving telescope
K_t	0.5	/	transmitting optical system efficiency
K_r	0.2	/	receiving optical system efficiency

Figure 6 shows the position of the sun and the earth, when the penumbra lunar eclipse occur. According to the orbital dynamics, the earth blocked part of the sun and the moon entered the earth's penumbra, in which time the temperature of the moon surface decreased. The LLR experiment recorded the change of effective echo rate when CCRs entered and left the penumbra of the earth, as shown in Fig. 7. The abscissa represents time and the ordinate represents the ranging residual. By analyzing Fig. 7, it is obtained that the effective echo rate of the CCRs in the penumbra of the earth is larger than that of its absence. The average effective echo rate and peak effective echo rate statistics of L2 are collected, as shown in Fig. 8. In Fig. 8, four groups of experimental results are recorded, of which two groups are corner reflectors in the penumbra of the earth and two groups are out of penumbra. Table 3 records the distance measurement for the L2 from 19:00 to 21:00. When L2 is in the penumbra of the earth, the average effective echo rate is revealed to reach 0.02 photons/s, and that at the peak effective echo rate is 0.18 photons/s. In particular, due to the deformation of the CCRs, we will no longer be able to get effective echo signals, when L2 removes out of the penumbra 11 minutes later. In particular, compared with the previous L2 full moon period experimental data, the effective echo rate is significantly enhanced. When L2 CCRs are moving out of the penumbra of the earth, its average effective echo rate experiences a downward trend, as shown in Fig. 9(a). Figure 9(a) shows the statistics of effective echo rate after L2 leaves the earth penumbra for 10 minutes. It results that the effective echo rate of L2 decrease fast, and shows an exponential law. Finally, the effective echo rate is reduced by 2 orders of magnitude. Figure 9(b) shows the relationship between received energy and dihedral angle errors. From the theoretical calculation, it can be obtained that the received energy decreases with the increase of dihedral angle errors. When the dihedral angle errors reach 1″, the energy intensity of the energy decreases by 2 orders of magnitude as compared with that without the dihedral angle errors. The theoretical calculation matches the experimental results.

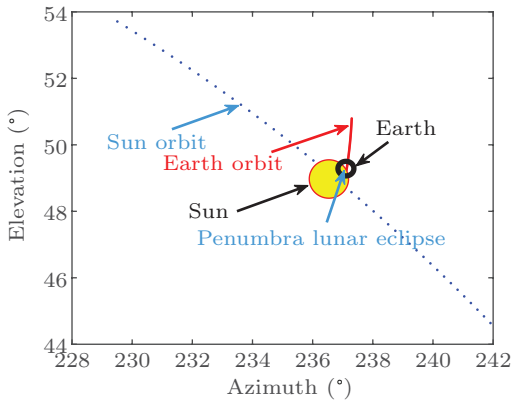


Fig. 6. Penumbra lunar eclipse. The orbits of the sun, the earth and their respective positions during the penumbra lunar eclipse. The blue point represents the solar orbit, and the red point refers to the earth's orbit. The black circle is the earth, and the yellow disk is the sun. The overlapping part indicate the occurrence of a penumbra lunar eclipse.

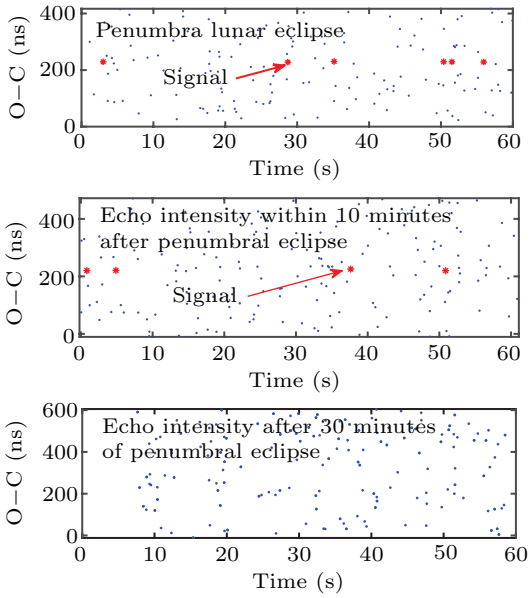


Fig. 7. Residuals of LLR. Red dots represent echo signals and blue dots represent noise. The top picture shows L2 is in the penumbra of the earth. The middle picture illustrates the signal intensity of L2 moving out of the penumbra of the earth within 10 minutes. The bottom picture shows the signal intensity 30 minutes after L2 is removed from the penumbra of the earth.

Table 3. LLR experiment.

Target	Start time (UTC)	End time (UTC)	Average effective echo rate	Peak effective echo rate	Penumbra lunar eclipse
L2	11:00	11:10	0.01 photons/s	0.1 photons/s	in
	11:20	11:30	0.02 photons/s	0.18 photons/s	in
	12:05	12:07	×	×	out
	12:20	12:23	×	×	out

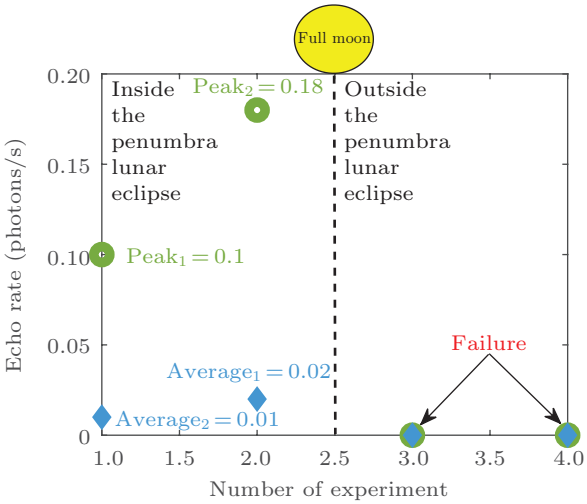


Fig. 8. Statistics of effective echo rate of LLR. Blue quadrilateral presents the average effective echo rate and green circle refers to the peak effective echo rate.

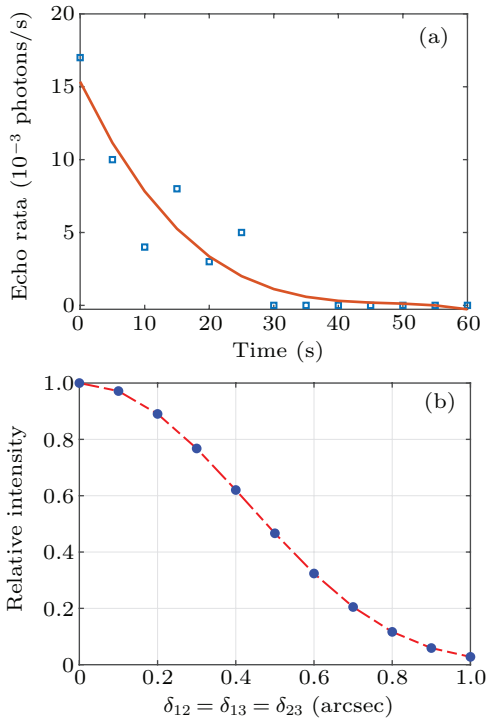


Fig. 9. (a) Effective echo rate of L2 after leaving the penumbra of the earth for 10 minutes. The abscissa represents the experiment time and the ordinate represents the effective echo rate. The blue square represents the experimental effective echo rate, and the red curve is the fitting result of the experimental data. (b) Theoretical calculation of relation between relative intensity and dihedral angle errors.

6. Conclusion

On September 27, 1996 and November 21, 2010, the OCA Observatory in France and the Apache Point station in the United States performed LLR experiment under lunar eclipse conditions. The main targets of their measurement and analysis were the Apollo series CCRs. The Apache Point Observatory focused on the influence of thermal gradients on the energy distribution of FFDP. Being different from Apache Point Observatory, this paper focuses on the measurement and analysis of the effective echo intensity of the L2 CCRs under the condition of the penumbra lunar eclipse, and calculates the influence of dihedral angle errors on FFDP. It concludes that when the dihedral angle errors is 1″, the energy will decrease 100 times. In the experiment, it is found that after CCRs are moved out of the penumbra 10 minutes, effective echo begins to decline rapidly, and the decline trend shows exponential law. In a very short time interval, the effective echo rate decreases by two orders of magnitude. Finally, the signal will disappear 11 minutes after the CCRs leave penumbra. We believe that dihedral angle errors ultimately affect the echo energy of L2.

Acknowledgements

We are very grateful to Rui Ge and Biao Zhang from Nanjing University for their help installing and debugging the SNSPDs. Thanks to Huizhong Duan from Sun Yat-sen University for his contributions in theoretical direction.

Project supported by the National Natural Science Foundation of China (Grant No. 12033009).

References

[1] Biskupek L and Torre J M 2021 *Universe* **7** 34
[2] Williams J G, Dicke R H, Bender P L, Alley C O and Wilkinson D T 1976 *Phys. Rev. Lett.* **36** 551
[3] Yi X and Kopeikin S 2010 *Proceedings of the International Astronomical Union* **5**(S261) 350
[4] Bender P L, Currie D G, Poultney S K, Alley C O, Dicke R H, Wilkinson D T, Eckhardt D H, Faller J E, Kaula W M and Mulholland J D 1973 *Science* **182** 229
[5] Hammond A L 1970 *Science* **170** 1289
[6] Shelus P J 1985 *IEEE Transactions on Geoscience and Remote Sensing* **GE-23** 385
[7] Li Y Q, Fu H L, Li R W, Tang R F, Li Z L, Zhai D S, Zhang H T, Pi XY, Hsienchi Yeh and Xiong Y H 2019 *Chin. J. Laser.* **46** 0104004
[8] Courde C, Torre J M, Samain E, Martinot-Lagarde G and Viswanathan V 2017 *Astron. Astrophys* **602** A90
[9] Battat J B R, Murphy T W, Adelberger E G, Gillespie B, Hoyle C D, Mcmillan R J, Michelsen E L, Nordtvedt K, Orin A E and Stubbs C W 2017 *Publications of the Astronomical Society of the Pacific* **129** 049201
[10] Murphy Jr T W, Adelberger E G, Battat J B R, Hoyle C D and Swanson H E 2012 *Classical Quant. Grav.* **29** 184005
[11] Murphy T W 2013 *Rep. Prog. Phys.* **76** 076901

[12] Murphy T W, Michelson E L, Orin A E, Adelberger E G, Hoyle C D, Swanson H E, Stubbs C W and Battat J B 2007 *Int. J. Mod. Phys. D* **16** 2127
[13] Strasburg J D, Murphy Jr T W, Stubbs C W, Adelberger E G and Angle J I 2002 *Int. Soc. Opt. Photon.* **4836** 387
[14] Müller J, Murphy T W, Schreiber U, Shelus P J and Hofmann F 2019 *J. Geodesy* **93** 2195
[15] Murphy T W, Adeberger E G, Battat J B R, Hoyle C D, Johnson N H, Mcmillan R J, Michelsen E L, Stubbs C W and Swanson H E 2011 *Icarus* **211** 1103
[16] Goodrow S D and Murphy T W 2012 *Appl. Opt.* **51** 8793
[17] Murphy Jr T W, Mcmillan R J, Johnson N H and Goodrow S D 2014 *Icarus* **231** 183
[18] Currie D 2012 *Science* **71** 131
[19] Martini M, Dell'Agnello S and Currie D 2012 *Planetary and Space Science* **74** 276
[20] Araki H, Kashima S, Noda H, Kunimori H, Chiba K, Mashiko H, *et al.* 2016 *Earth, Planets and Space* **68** 1
[21] Zhou H, Li S, Zhang W H and Chen Y W 2020 *Appl. Opt.* **59** 2621
[22] He Y, Liu Q, He J J, Li M, Duan H Z and Hsien C Y 2018 *Chin. Phys. B* **27** 100701
[23] Wang J T, Zhou J, Zang H G and Zhu X L 2010 *Chin. Opt. Lett.* **8** 670
[24] Zhang H F, Long M L, Deng H R, Wu Z B, Cheng Z E and Zhang Z P 2019 *Chin. Opt. Lett.* **17** 051404
[25] Liu F, Jiang M S, Lu Y F, Wang Y and Bao W S 2021 *Chin. Phys. B* **30** 040302
[26] Zhou H, He Y H, Lv C L, You L X, Li Z H, Wu G, Zhang W J, Zhang L, Liu X Y, Yang X Y and Wang Z 2018 *Chin. Phys. B* **27** 018501
[27] Wang Y, Li H, You L X, Lv C L, Wang H Q, Zhang X Y, Zhang W J, Zhou H, Zhang L, Yang X Y and Wang Z 2019 *Chin. Phys. B* **28** 078502